



Originally published as:

Schwalenberg, K., Rippe, D., Koch, S., Scholl, C. (2017): Marine-controlled source electromagnetic study of methane seeps and gas hydrates at Opouawe Bank, Hikurangi Margin, New Zealand. - *Journal of Geophysical Research*, 122, 5, pp. 3334—3350.

DOI: <http://doi.org/10.1002/2016JB013702>

## RESEARCH ARTICLE

10.1002/2016JB013702

## Key Points:

- 1-D and 2-D inversions of marine CSEM data over active methane seeps and gas hydrate targets at Opuawe Bank, New Zealand
- Highly anomalous resistivity zones below gas seeps indicate high gas hydrate saturations
- Coexistence of gas hydrate and free gas below the seeps within the hydrate stability zone from joint CSEM and seismic interpretation

## Supporting Information:

- Supporting Information S1

## Correspondence to:

K. Schwalenberg,  
katrin.schwalenberg@bgr.de

## Citation:

Schwalenberg, K., D. Rippe, S. Koch, and C. Scholl (2017), Marine-controlled source electromagnetic study of methane seeps and gas hydrates at Opuawe Bank, Hikurangi Margin, New Zealand, *J. Geophys. Res. Solid Earth*, 122, 3334–3350, doi:10.1002/2016JB013702.



Received 11 NOV 2016

Accepted 31 MAR 2017

Accepted article online 17 APR 2017

Published online 27 MAY 2017

## Marine-controlled source electromagnetic study of methane seeps and gas hydrates at Opuawe Bank, Hikurangi Margin, New Zealand

Katrin Schwalenberg<sup>1</sup> , Dennis Rippe<sup>1,2</sup>, Stephanie Koch<sup>3</sup> , and Carsten Scholl<sup>4</sup>

<sup>1</sup>BGR Federal Institute for Geosciences and Natural Resources, Hannover, Germany, <sup>2</sup>Now at GFZ Helmholtz Centre Potsdam, German Research Centre for Geosciences, Potsdam, Germany, <sup>3</sup>GEOMAR Helmholtz Centre for Ocean Research, Kiel, Germany, <sup>4</sup>CGG Electro Magnetics GmbH, Berlin, Germany

**Abstract** Marine controlled source electromagnetic (CSEM) data have been collected to investigate methane seep sites and associated gas hydrate deposits at Opuawe Bank on the southern tip of the Hikurangi Margin, New Zealand. The bank is located in about 1000 m water depth within the gas hydrate stability field. The seep sites are characterized by active venting and typical methane seep fauna accompanied with patchy carbonate outcrops at the seafloor. Below the seeps, gas migration pathways reach from below the bottom-simulating reflector (at around 380 m sediment depth) toward the seafloor, indicating free gas transport into the shallow hydrate stability field. The CSEM data have been acquired with a seafloor-towed, electric multi-dipole system measuring the inline component of the electric field. CSEM data from three profiles have been analyzed by using 1-D and 2-D inversion techniques. High-resolution 2-D and 3-D multichannel seismic data have been collected in the same area. The electrical resistivity models show several zones of highly anomalous resistivities ( $>50 \Omega\text{m}$ ) which correlate with high amplitude reflections located on top of narrow vertical gas conduits, indicating the coexistence of free gas and gas hydrates within the hydrate stability zone. Away from the seeps the CSEM models show normal background resistivities between  $\sim 1$  and  $2 \Omega\text{m}$ . Archie's law has been applied to estimate gas/gas hydrate saturations below the seeps. At intermediate depths between 50 and 200 m below seafloor, saturations are between 40 and 80% and gas hydrate may be the dominating pore filling constituent. At shallow depths from 10 m to the seafloor, free gas dominates as seismic data and gas plumes suggest.

### 1. Introduction

Gas hydrates are naturally occurring ice-like solids storing large amounts of methane in a cage structure of water and gas molecules. They form at high pressure and low temperatures and have been identified worldwide in shallow seafloor sediments along continental margins. Present research interest in submarine gas hydrate is focused on the energy resource potential [Boswell and Collett, 2011] as the global amount of carbon stored in submarine hydrates is vast and likely exceeds the total amount of conventional hydrocarbon resources including oil, gas, and coal [e.g., Kvenvolden, 1993; Milkov, 2004].

Of particular interest are areas of enhanced fluid flow and methane seepage from deepwater sediments which are often found along compressive margins and have been associated with the formation of locally higher gas hydrate concentrations [e.g., Collett et al., 2009; Piñero et al., 2013]. These seep structures are characterized by the migration of methane-rich fluids and/or free gas along subvertical faults and fissures into the gas hydrate stability zone (GHSZ). Gas plumes in the water column and seepage-related ecosystems indicate where the seep structures reach the seafloor.

Geophysical methods have been commonly used to identify and assess the resource potential of gas hydrates in the subseafloor. Electrical resistivity data derived from marine controlled source electromagnetics (CSEM) are sensitive to the sediment porosity and the electrical properties of the pore fluid. In particular, the replacement of conductive seawater with resistive gas or gas hydrate increases the formation resistivity [e.g., Edwards, 1997] which can be used to derive volume saturation estimates. Carbonates that have formed at active seep sites are also resistive and may increase the formation resistivity. Reflection seismic and hydroacoustic data provide structural images of subseafloor gas migration pathways and the presence of gas hydrate, both causing scatter and blanking of seismic signals [e.g., Riedel et al., 2002; Wood et al., 2008; Plaza-Faverola et al., 2012]. Seismic velocity data also distinguish between gas hydrate (higher velocity)

and free gas (lower velocity) and have been used to estimate gas hydrate saturations [e.g., Wood *et al.*, 1994; Yuan *et al.*, 1996].

The combination of electrical resistivity and seismic data has demonstrated great use for the identification and evaluation of submarine gas hydrate reservoirs in boreholes [e.g., Paull *et al.*, 2000; Tréhu *et al.*, 2006; Riedel *et al.*, 2005; Expedition 311 Scientists, 2006; Shankar and Riedel, 2014] and in an increasing number of area-wide operating geophysical field studies [Yuan and Edwards, 2000; Schwalenberg *et al.*, 2005, 2010a, 2010b; Weitemeyer *et al.*, 2006, 2011; Weitemeyer and Constable, 2010; Ellis *et al.*, 2008; Goto *et al.*, 2008; Goswami *et al.*, 2015; Constable *et al.*, 2016]. Simple rock physics models [e.g., Hashin and Shtrikman, 1962; Archie, 1942] have been applied to estimate the amount of gas or gas hydrate within the sediments. These models demonstrate that high saturations of either free gas or gas hydrate (>50%) are required to increase the formation resistivity typically from values around 1  $\Omega\text{m}$  to values closer to 3  $\Omega\text{m}$ . Smaller saturations on the order of <10% may not impact resistivity data or could be mistaken for lithological changes. In contrast, only a few percent of free gas and gas hydrate can alter seismic signals and velocities. Thus, the combination of seismic and CSEM methods allows better quantification of free gas and gas hydrate accumulations and improves the understanding of their distribution in the subsurface.

Here we present a case study by using marine CSEM data and reflection seismic imaging to investigate gas seep structures and related gas hydrate deposits at Opouawe Bank, New Zealand. The CSEM data have been acquired by using a newly developed, seafloor-towed, electric dipole-dipole system designed to image the subseafloor sediment section where gas hydrate typically occurs. 1-D and 2-D inversion techniques have been applied to the CSEM data to derive the electrical resistivity distribution and to estimate the free gas and gas hydrate concentration below the seeps. The CSEM results show that large volumes of resistive material (i.e., both gas and gas hydrate) have accumulated below the seeps which was not clear from seismic data alone and also demonstrates that these features may have particularly high resource potential.

## 2. Study Area

Opouawe Bank is located at the Hikurangi Margin off the east coast of New Zealand's North Island (Figure 1) which marks the southern end of the Tonga-Kermadec-Hikurangi subduction zone where the Pacific plate is subducting westward beneath the Indo-Australian plate [Walcott, 1978]. The central part of the Hikurangi Margin is characterized by accretion of 500–2000 m thick marine sediments of Pliocene to Quaternary age [Davy and Wood, 1994]. These sediments lie on top of the 12–15 km thick crust of the Hikurangi Plateau which consists of mid-ocean ridge basalts of pre-Tertiary age. The slope of the accreted sediment is generally less than 4°, suggesting low friction at the plate interface, presumably the result of high water content in the sedimentary layer [Barnes *et al.*, 2010].

Methane seepage on the Hikurangi Margin was first described by Lewis and Marshall [1996] based on evidence from seep faunas, bubble plumes, carbonate crusts, and bacterial mats. The presence of submarine gas hydrate on Hikurangi Margin has been inferred from widespread bottom-simulating reflectors (BSRs) in reflection seismic data representing the base of the gas hydrate stability zone (GHSZ) [Townend, 1997; Katz, 1982; Henrys *et al.*, 2003; Pecher *et al.*, 2004] and through direct sampling of gravity cores collected within the NEW VENTS and NEMESYS projects during R/V SONNE cruises SO191 and SO214 [Bialas *et al.*, 2007; Bialas, 2011; Schwalenberg *et al.*, 2010a].

### 2.1. Opouawe Bank

An area of particular interest within these projects was Opouawe Bank located offshore the Wairarapa coast (Figure 1). It is part of the ridge and basin systems of the accretionary wedge of the subduction zone. SW-NE striking Opouawe Bank is about 20 km  $\times$  10 km in size and located in 1000–1100 m water depth. So far, 14 seep sites have been found at Opouawe Bank [Greinert *et al.*, 2010].

Most seep sites are aligned along the ridge crest. Repeated observations of methane plumes in hydroacoustic data indicate active venting. Video observations, high-resolution deep-towed side scan, and sub-bottom profiler data [Klaucke *et al.*, 2010; Dumke *et al.*, 2014] show outcrops of authigenic carbonates indicating that seafloor venting has been active for some time. Multichannel seismic (MCS) reflection studies conducted as part of the NEW VENTS project found the BSR at Opouawe Bank at 0.5–0.6 s two-way travel time below seafloor [Netzeband *et al.*, 2010; Barnes *et al.*, 2010]. High-resolution 2-D MCS and low-frequency sediment

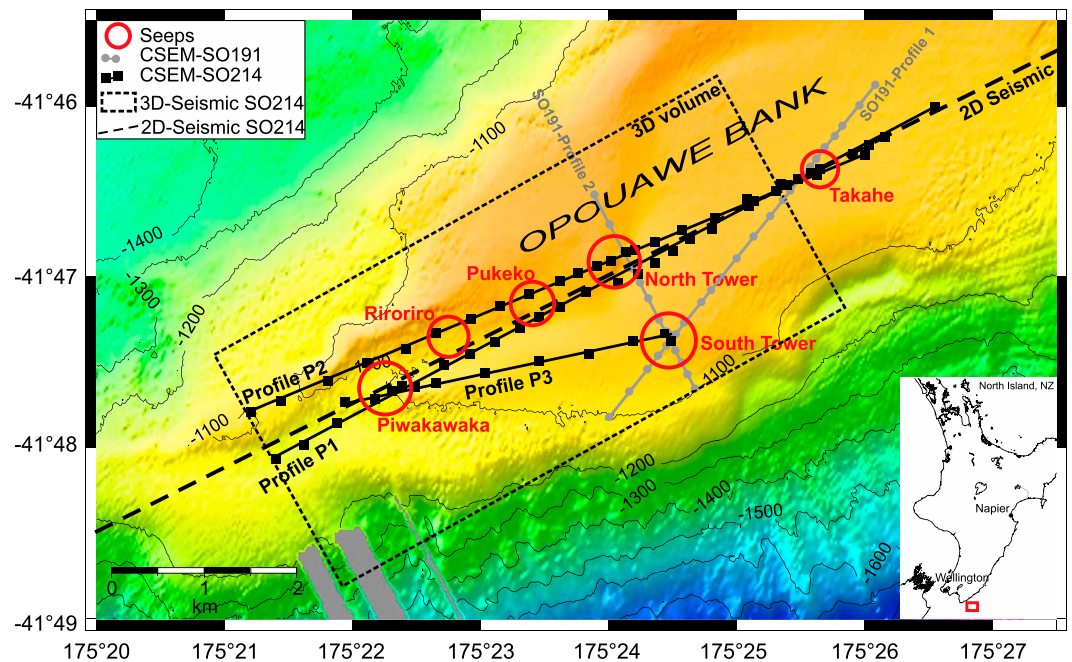


**Figure 1.** Map of the southwestern part of Opoouawe Bank located in water depth from 1000 to 1100 m. The red circles indicate seep site locations. The black squares and lines are waypoints along CSEM profiles P1, P2, and P3 used in this study. The gray lines are CSEM profiles published in *Schwalenberg et al.* [2010a]. The dotted rectangle marks the outline of the 3-D seismic volume and the dashed line the 2-D MCS line.

echo sounder data reveal subvertical gas migration structures beneath all seep sites and horizontal strata away from the seeps. They present conduits for essentially pure methane through the GHSZ [*Koch et al.*, 2016]. The conduits are characterized by high amplitude reflection anomalies, acoustic turbidity, blanking, and upward bending of reflections at different levels [*Netzeband et al.*, 2010]. *Krabbenhoft et al.* [2013] proposed that seepage at Opoouawe Bank is structurally driven and parts of the upward migrating gas form gas hydrate resulting in a higher gas/gas hydrate saturation below the seeps. So far, the only gas hydrate samples at Opoouawe Bank have been retrieved from shallow gravity cores at Takahe seep site [*Luo et al.*, 2016; *Bialas*, 2011; *Schwalenberg et al.*, 2010a].

Analysis of new sediment echo sounder, 2-D and 3-D MCS data collected during cruise SO214 of R/V *SONNE*, provides further evidence of free gas entering the GHSZ [*Koch et al.*, 2015, 2016]. 3-D seismic images show that the gas conduits in fact are narrow elongated fracture systems perpendicular to the ridge axis [*Koch*, 2016]. Velocity data derived from 2-D industry-style, long-offset MCS data disclosed a low-velocity zone (LVZ) at BSR level and dipping high amplitude reflections crossing the BSR at the LVZ indicating traps of upward migrating free gas at the base of the GHSZ [*Plaza-Faverola et al.*, 2012; *Koch et al.*, 2016].

Earlier marine CSEM data collected in 2007 as part of the NEW VENTS project [*Schwalenberg et al.*, 2010a; *Bialas et al.*, 2007] revealed highly anomalous resistivities beneath the North Tower and South Tower seep sites (Figure 1) and have been assigned to locally higher gas hydrate saturations. Takahe, a smaller seep site, yielded only slightly elevated resistivities which have been explained by patchy gas hydrates and gas pockets.

In summary, Opoouawe Bank is an area of active seafloor venting indicating a high supply of biogenic methane from below the BSR into the GHSZ [*Koch et al.*, 2016]. Hydroacoustic and seismic data provide evidence that large amounts of free gas migrate through the GHSZ toward the seafloor and possibly form concentrated hydrate on top of the conduits. Highly anomalous resistivity zones beneath North Tower and South Tower, inferred by our previous CSEM experiments, have been explained with locally enhanced gas hydrate saturations. Away from the seeps seismic, hydroacoustic and CSEM data show normal layering and background values with no indication for methane seepage.



### 3. Materials and Methods

A summary of the basic theory of marine time domain CSEM methods can be found in *Cheesman et al.* [1987] and *Edwards* [1997, 2005]. Based on their high resistivities, *Edwards* [1997] suggested the use of time domain CSEM data for the detection of submarine gas hydrates. Several gas hydrate exploration case studies followed using CSEM systems in time domain [*Yuan and Edwards*, 2000; *Schwalenberg et al.*, 2005, 2010a, 2010b], frequency domain [*Weitemeyer et al.*, 2006, 2011; *Weitemeyer and Constable*, 2010; *Ellis et al.*, 2008; *Constable et al.*, 2016; *Goswami et al.*, 2015, *Attias et al.*, 2016], and a DC resistivity system [*Goto et al.*, 2008].

#### 3.1. CSEM Instrumentation

The marine CSEM data used in this study have been acquired with a newly developed, time domain, seafloor-towed, electric dipole-dipole system called HYDRA (Figure 2) which has been particularly designed for subseafloor gas hydrate assessments [*Schwalenberg and Engels*, 2011]. The system is an advancement in terms of data coverage and quality to the previous seafloor-towed CSEM system built at the University of Toronto which consisted of only two electric dipole receivers [*Yuan and Edwards*, 2000] and which was used during the NEW VENTS project on R/V *SONNE* cruise SO191 [*Schwalenberg et al.*, 2010a, 2010b]. HYDRA is a modular system consisting of four electric receiver dipoles towed at offsets from 160 m (R1) to 754 m (R4) behind a 100 m long transmitter dipole (TX), thus measuring inline components of the horizontal electrical field (Figure 2). The system is typically sensitive to structure up to about 300 m below the seafloor. A heavy weight ("pig") is attached to the front of the seafloor array. It hosts the control unit which also records the transmitted source signal, a CTD (conductivity, temperature, and density) sensor to measure seawater conductivities and pressure that provides water depths, and an acoustic transponder to locate the seafloor instrument. A current-controlled transverter located on board the research vessel was used, capable to transmit currents up to 13 A at 1000 V but was limited by the resistance of the deep-tow coaxial cable and slip-rings to a maximum peak-to-peak amplitude of  $I = \pm 6$  A. The transmitted source signal had a square waveform with 100% duty cycle and a period of 6 s (see Figure S1 in the supporting information).

The four receiving dipoles were between 10 and 20 m long with a pair of Ag/AgCl electrodes on either end. Each RX dipole was connected to a battery-powered receiver unit which includes low noise front end electronics, a 22 bit analog-to-digital converter, a data logger, and a high-precision oven-heated oscillator clock. Data were sampled at 10 kHz and stored locally at each receiver unit on Secure Digital cards. Online communication and data transfer between the deck unit and the seafloor array during deployments were not yet realized; thus, data were downloaded after instrument recovery.

#### 3.2. Surveying

HYDRA was deployed by using the vessel's aft A-frame and aligned on the seafloor paying out the deep-tow cable while moving the ship along the profile. A cable length of 3 times the water depths was used to tow the array behind the ship. To collect high-quality data the ship was kept stationary every 150 m to 500 m for about 10 min, while an additional cable length of 300 m was paid out to avoid movement of the array during measurements on-site. This extra length was reeled in before the ship moved to the next waypoint. Even though this procedure considerably slows down the survey and risks damage to the instrument while towing on the seafloor, the recorded time series show high data quality and allow higher stacking to improve signal-to-noise ratios and denser spacing over areas of particular interest (Figures S1 and S2). It is common procedure to calibrate the HYDRA system while the complete array was hanging vertically in the water in the beginning and end of the deployment but, unfortunately, these data were noisy due to receiver electrodes moving in the water and could not be used.

#### 3.3. Data Processing

Matlab scripts have been composed to process the CSEM data. The recorded time series of all receivers were visually inspected, and time intervals were selected while the array was stationary at each waypoint. A zero-phase Butterworth low-pass filter with a cut-off frequency equal to the Nyquist frequency of the decimated time series (here 1250 Hz) was applied to reduce internal high-frequency noise from the electronics. The transmitter and receiver time series were then decimated from the original sampling rate of 10 kHz to 2500 Hz which also has the effect of a low-pass filter. Gain, DC-offset, and drift corrections were applied to the data, and the time series intervals at each waypoint were divided in 3 s long half-periods.

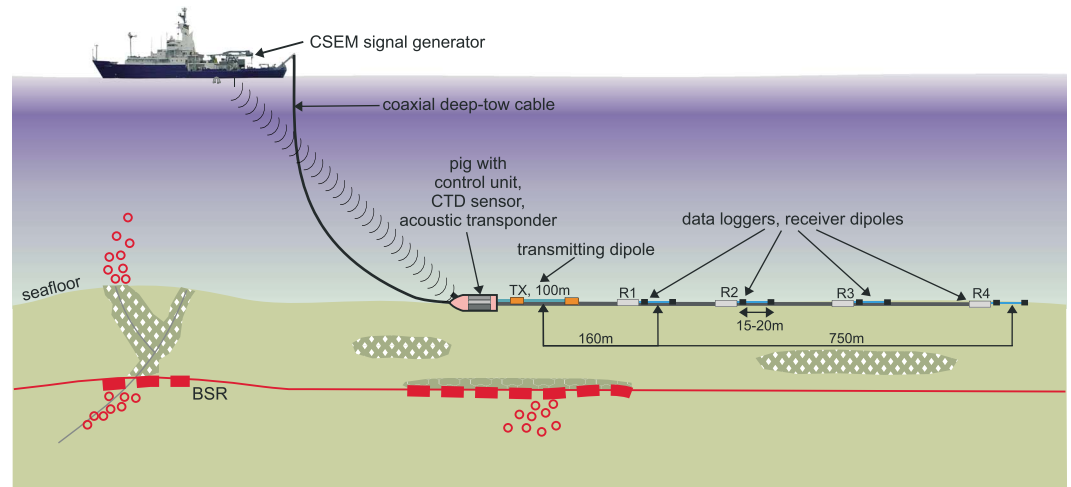


**Figure 2.** Configuration of the seafloor-towed HYDRA system used during the SO214 expedition. The system consists of a 100 m long transmitting dipole and four receiving dipoles towed at increasing offsets from 160 m to 754 m. The pig is a heavy weight hosting the control unit, a CTD sensor, and an acoustic transponder.

We analyzed the data by using 1-D inversion in time domain and 2-D inversion in frequency domain. For data analysis in time domain a stacked data set was derived from the selected half-periods by using an iterative stacking scheme (Figure S2). Data errors were calculated from the standard deviation of each stack.

For data analysis in frequency domain, the half-periods of both transmitter and receiver data were transformed into frequency domain via fast Fourier transformation and real and imaginary parts were calculated from band-pass filtered auto- and cross correlations. Data errors were estimated by using a Fisher distribution (Figure S3).

## 4. Results

CSEM data have been analyzed along three profiles intersecting most of the known seep sites at Opuawe Bank (Figure 1). Profile P1 is oriented in NE-SW direction and intersects seeps Takahe, North Tower, Pukeko, and Piwakawaka. Profile P2 crosses seeps Takahe, North Tower, Pukeko, and Riroriro. Profile P3 runs in ESE to WNW direction and intersects with Profile P1 at Piwakawaka and covers parts of South Tower. The map also shows the 2-D MCS line and the area surveyed with the P-cable 3-D seismic system during cruise SO214 [Bialas, 2011].

### 4.1. 1-D Inversion

In a first step we applied the 1-D inversion program *MARTIN* provided by C. Scholl (University of Toronto, 2007, unpublished software) to calculate apparent resistivity profiles for each receiver. The program uses either Marquardt- [Marquardt, 1963] or Occam-type inversion techniques [Constable et al., 1987] to determine the subsurface resistivity structure.

The objective function for the Occam-type inversion can be expressed as

$$\varphi = (\mathbf{d} - \mathbf{f}(\mathbf{m}))^T \mathbf{W}^2 (\mathbf{d} - \mathbf{f}(\mathbf{m})) + \beta (\lambda_R \mathbf{Rm}^T \mathbf{Rm} + \lambda_{CF} \mathbf{m}^T \mathbf{I}_{CF} \mathbf{m}). \quad (1)$$

Here  $\mathbf{d}$  is the data vector,  $\mathbf{m}$  the model vector,  $\mathbf{f}(\mathbf{m})$  the forward operator,  $\mathbf{W}$  a diagonal weighting matrix with the inverse of the error estimates on its main diagonal,  $\mathbf{R}$  a roughness matrix as described in Constable et al. [1987], and  $\beta$  is the trade-off parameter between data fit and model roughness.  $\mathbf{I}_{CF}$  is a square matrix that has entries only on the main diagonal relating to the calibration factor (CF), and  $\lambda_R$  and  $\lambda_{CF}$  are scalars that are used to balance the two parts of the regularization term.  $\beta$  acts on both parts of the regularization term and is the only parameter that the inversion changes itself, while  $\lambda_R$  and  $\lambda_{CF}$  are set in a series of test runs with the goal to reach a minimum misfit and keeping the regularization strong. The calibration factors (CFs) are part of the model vector  $\mathbf{m}$ . They are multiplied by the model responses and compensate for unknown

errors such as geometry, unexpected time delays between the transmitter and receiver unit clocks, or 2-D and 3-D effects in the data [Hoerdt and Scholl, 2004; Commer and Newman, 2008]. Ideally, the calibration factor is equal or close to 1.

For Marquardt-type inversion equation (1) is reduced to the first term on the right-hand side corresponding to the data misfit and a  $\beta$ -controlled damping term.

The inversion progress is controlled by the root-mean-square (RMS) misfit which is here defined as

$$\text{total RMS} = \sqrt{\frac{1}{N} \sum_i \left| \frac{(d_i^{\text{obs}} - d_i^{\text{calc}})^2}{(f_i \sigma_i)^2} \right|} \quad (2)$$

where  $N$  is the number of observations, i.e., data;  $d_i^{\text{obs}}$  are the measured data from all receivers considered in the inversion;  $d_i^{\text{calc}}$  are the model responses;  $\sigma_i$  are the data errors derived from the standard deviations of the stacked half-periods at each site; and  $f_i$  are scaling factors applied to the data errors. The inversion terminates if a total RMS of 1 or less is reached, which means that the fit is within the statistically data error or no better model update can be found. The total RMS misfit is the mean of individual receiver RMS misfits, which can be higher or lower than 1. A single RMS value can lead to bias the inversion as parts of the data would be up- or down-weighted. This problem can be tackled by scaling the data errors with  $f_i$  to yield individual receiver misfits close or equal to 1.

#### 4.1.1. Apparent Resistivity Profiles

Marquardt inversion was used to calculate the apparent resistivity at each site along the three profiles from simple half-space starting models and fixed water depth and seawater conductivities. This provides a first overview of the average resistivity distribution shown in Figure 3. Apparent resistivity values are clearly anomalous ( $>10 \Omega\text{m}$ ) at the western seep sites (Piwakawaka, Riroriro, Pukeko, North Tower, and South Tower), while normal background resistivities of 1.16–1.64  $\Omega\text{m}$  have been derived away from the seep sites. At Takahe to the east, resistivities are slightly elevated at receiver R1 on profile P2.

Penetration depth increases with receiver offset; thus, the apparent resistivity profiles already indicate whether the anomaly is located closer to the seafloor ( $\rho_a$  is highest for R1 at 160 m offset, e.g., Pukeko on profile P2) or deeper within the GHSZ ( $\rho_a$  is highest for R3 and R4 at 405 m and 610 m offsets, e.g., Riroriro on profile P2). Calibration factors (CFs) and RMS misfits are close to 1 at most sites and high above the seeps which we attribute to 2-D and 3-D effects in the data.

Figure 3 also indicates that at several sites, data from some receivers are missing which was due to drifts of the receiver electrodes. Along profile P1, data from R1 are only available at the eastern end of the profile. Between 3200 m and 4200 m along profile, data from R4 are missing, as well as at the western end from R2 (0–1900 m) and R3 (0–1000 m). For profiles P2 and P3 no data from R2 are available. Data from R1 are missing after profile meter 1000 on profile P3. Note, the original tow direction was NE to SW along P1 and P2 and SW to NE along P3.

#### 4.1.2. 1-D Occam Inversion

Multilayered 1-D Occam inversions have been conducted to obtain constraints on the vertical resistivity structure by using starting models with 20 layers of logarithmically increasing thicknesses. Water depths and seawater conductivities were taken from the CTD sensor and are fixed parameters in the inversion. The individual 1-D layered resistivity models were derived from joint inversion of all available transmitter-receiver pairs at each site and have been assigned to the midpoint between the transmitter dipole and the dipole of receiver R3 at 405 m offset. The 1-D models have been stitched together laterally for a 2-D presentation (Figures 4a–4c, bottom row). All three profiles show highly anomalous resistivities ( $>10 \Omega\text{m}$ ) below the western seep sites within the top 200 mbsf (meters below seafloor) compared to relatively homogeneous background resistivities of 1–2  $\Omega\text{m}$  away from the seep sites. At greater depths, the models show anomalously low resistivities ( $<1 \Omega\text{m}$ , dark red colors) which we attribute to be numerical artifacts caused by 2-D or 3-D effects around the seeps and to topography effects at North Tower. Calibration factors and total RMS misfits are  $>1$  at Pukeko and North Tower where topography and 3-D effects are strongest and a 1-D interpretation fails and close to 1 elsewhere. Individual receiver RMS misfits are generally balanced around 1 when applying scaling factors  $f_i = [1.0, 0.8, 0.7, 0.5]$  for R1, R2, R3, and R4, respectively (Figure 4, top row). Time domain data and data fit of the models in Figure 4 are shown in Figure S4.

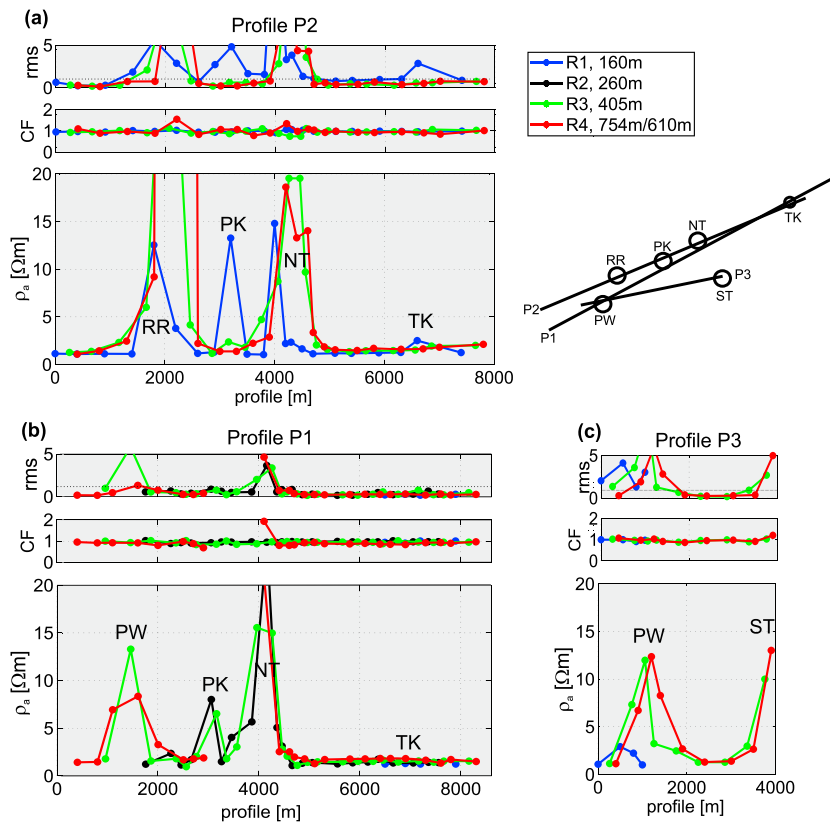


**Figure 3.** (bottom row) Apparent resistivity profiles, (top row) RMS misfit, and (middle row) calibration factors (CFs) for all available receivers along profiles (a) P2, (b) P1, and (c) P3 derived from Marquardt inversion. Missing receiver data are due to electrode drift. Offsets to R4 were 754 m for P1 and 610 m for P2 and P3. Sketch top right depicts the position of the profiles and the seep sites Takahahe (TK), North Tower (NT), Pukeko (PK), Riroriro (RR), Piwakawaka (PW), and South Tower (ST); see also Figure 1 for locations. Highly anomalous apparent resistivities clearly correlate with the seep site locations. RMS misfits are high over the seeps indicating limitations of the half space interpretation. Calibration factors are generally close to 1.

**4.2. 2-D Occam Inversion**

We used the 2-D finite difference, Occam-type inversion algorithm *OTZE* by C. Scholl (CGG Electro Magnetics, proprietary software) to determine 2-D images of the subseafloor resistivity distribution. The program solves an objective function that equates the formula in equation (1). It allows anisotropic inversion with vertical transverse isotropy, taking account of the regional bathymetry along the profiles with the depth and dip of the transmitter and receivers being adjusted, accordingly. Figure 5 shows the inverted vertical resistivity models of the three profiles by using all available transmitter-receiver pairs. On top of the models the lateral coverage of available receiver data is displayed.

The 2-D inversion reveals areas of highly elevated electrical resistivities (>50 Ωm) at the western seep sites within the top 200 mbsf which is consistent with the 1-D inversion results in Figure 4. No unrealistically low resistivities appear at the deeper parts below the seeps in contrast to the 1-D inversions, supporting our assumption that these features are limitations of the 1-D inversion. Takahahe seep site to the east occurs as a small anomaly at profile meter 6900 in profile P2 (Figure 5a), a result that is consistent with Schwalenberg *et al.* [2010a].

Away from the seeps the resistivities are much lower, but the models show a three-layer case of conductive shallow sediments (1.1–1.4 Ωm), followed by a more resistive layer (2.0–2.2 Ωm) at about 150 mbsf and again lower resistivities (1.4–1.8 Ωm) at depth >250 mbsf. We think this could be caused by a change in lithology and subsequently in porosity supported by the prominent subhorizontal reflectors visible in the seismic sections (Figures 8 and S7-1). Also, a gas hydrate layer of moderate concentration would be plausible. Another explanation could be that more structure is introduced in the model by the inversion to reach a total RMS of 1 and the data are actually over-fit. The 1-D Occam inversion results in Figure 4 show that the

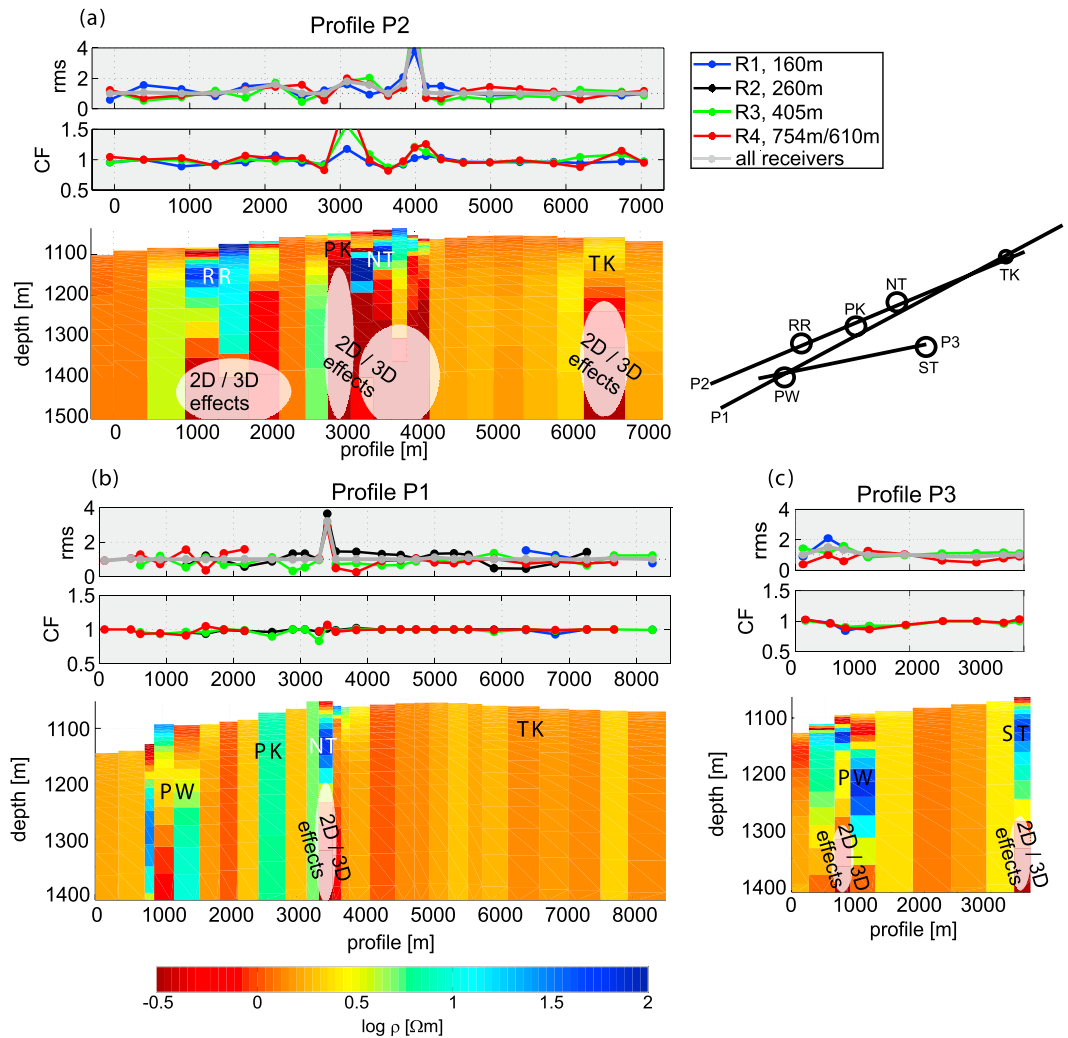


**Figure 4.** (bottom row) Stacked 1-D Occam inversion results, (top row) RMS misfit, and (middle row) calibration factors (CFs) for all available receivers along profiles (a) P2, (b) P1, and (c) P3. Sketch top right depicts the relative position of the profiles and the seep sites Takahe (TK), North Tower (NT), Pukeko (PK), Riroriro (RR), Piwakawaka (PW), and South Tower (ST). Highly anomalous resistivities not only clearly correlate with the seep site locations but also show high conductivities (above seawater) in the deeper parts which are due to 2-D and 3-D effects around the seep structures. Away from the seeps the resistivities have normal background values around 1–2 Ωm. RMS misfits of individual receivers are generally balanced around 1 for all receivers after error scaling with factors  $f_i = [1, 0.8, 0.7, 0.5]$  for R1, R2, R3, and R4. Calibration factors are also close to 1 except the seep sites at profile P2.

background sites away from the seeps could also be explained with a predominantly homogeneous resistivity structure.

All three models obtained from joint inversion of all available receivers have acceptable total RMS misfits of 1.31 (P1), 1.18 (P2), and 1.12 (P3). However, RMS misfits of individual receivers show values greater or smaller than 1.0 along the profiles (Figure 5, top row). Thus, the inversion process may be biased toward areas with higher data coverage and better data quality. Even though the data coverage is not homogeneous along the three profiles, the resistivity anomalies particularly below the western seep sites are well constrained, first-order features in the models, and are also confirmed by the data (see Figure S5).

### 5. Saturation Estimates

One objective of the CSEM study is to estimate the free gas and gas hydrate saturation that may have accumulated below the seeps at Opouawe Bank. Both free gas and gas hydrates are electrically resistive



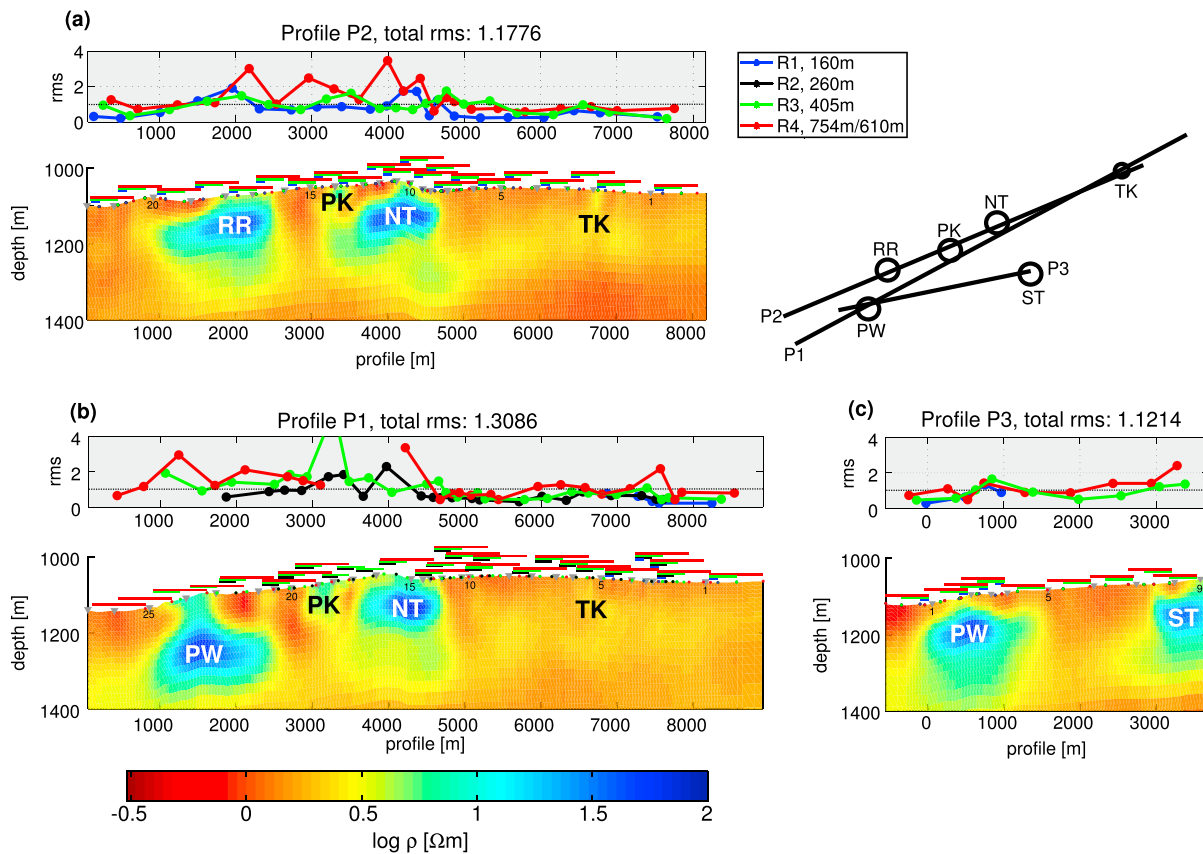


**Figure 5.** (bottom row) 2-D Occam inversion results and (top row) RMS misfit for all available receivers along profiles (a) P2, (b) P1, and (c) P3. On top of the three models the color-coded TX-RX offsets of all available receiver data are depicting the data coverage along the profiles (R1: blue, R2: black, R3: green, R4: red). Calibration factors are close to 1 along all profiles and not shown here. Sketch top right shows the relative position of the profiles and the seep sites Takaha (TK), North Tower (NT), Pukeko (PK), Riroriro (RR), Pihakawaka (PW), and South Tower (ST). At the western seep sites all three models show extended zones of highly anomalous resistivities (>50 Ωm) within the first 100–200 m below the seafloor. Takaha seep to the east shows slightly elevated resistivities at profile P2. Away from the seeps the resistivities have background values around 1–2 Ωm. Total RMS misfits are between 1.1 and 1.3 but show stronger undulations along the single receiver RMS profiles.

and cannot be distinguished from resistivity data alone. Authigenic carbonates that precipitate at active cold vents at the seafloor are also resistive but cover only patchy and isolated areas at Opuawe Bank [Klaucke et al., 2010] and are therefore not further considered.

Archie's law [Archie, 1942] has been the most commonly used approach to derive the gas hydrate/free gas saturation from borehole resistivity data [e.g., Collett and Ladd, 2000; Tréhu et al., 2006; Expedition 311 Scientists, 2006] and also from marine CSEM surveys [Schwalenberg et al., 2005, 2010a; Weitmeyer et al., 2006, 2011; Ellis et al., 2008; Goswami et al., 2015]. Cook et al. [2010] showed that saturation estimates derived from borehole resistivity logs via Archie's equation can be severely overestimated when hydrate has formed in fissures and fractures causing electrical anisotropy. Here we use Archie's law [1942] to derive average saturation estimates of large sediment volumes in the order of tens to hundreds of meters covered by CSEM data where we assume that the gas hydrate and free gas distribution is rather pore-filling on average.

Archie's empirical porosity-resistivity relation for a two-phase porous system of sediment grains and pore fluids is given by

$$\rho_0 = a \rho_w \phi^{-m} \tag{3}$$

where  $\rho_0$  is the formation resistivity of the pore water saturated sediment (i.e., background resistivity),  $\rho_w$  is the electrical resistivity of the pore fluid,  $\phi$  the sediment porosity,  $a$  is an empirical constant (tortuosity constant), and  $m$  is the cementation factor. If a third resistive phase is present, i.e., gas or gas hydrate, equation (3) can be generalized to

$$\rho_{gh} = a \rho_w S_w^{-n} \phi^{-m} \quad (4)$$

where  $\rho_{gh}$  is the formation resistivity of a sediment volume containing gas and/or gas hydrate,  $S_w$  is the saturation of the pore fluid,  $n$  is the saturation exponent, and  $S_{gh} = (1 - S_w)$  is the saturation of the third resistive phase, accordingly. Thus, gas hydrate/free gas saturation estimates can be derived by using

$$S_{gh} = 1 - \left[ \frac{a \rho_w \phi^{-m}}{\rho_{gh}} \right]^{\frac{1}{n}} \quad (5)$$

Assuming that the lithology does not change between gas hydrate/gas-free sediment sections, equation (4) simplifies to

$$\rho_{gh} = \rho_0 S_w^{-n} \quad (6)$$

and equation (5) to

$$S_{gh} = 1 - \left[ \frac{\rho_0}{\rho_{gh}} \right]^{\frac{1}{n}} \quad (7)$$

accordingly. In this case the general form of Archie's law requires no knowledge about the sediment porosity and cementation factor but only requires that these parameters do not change in the presence of gas hydrates or free gas.

In the general case, saturation estimates by using equation (5) require knowledge of the pore water resistivity, the sediment porosity, and a set of Archie coefficients  $a$ ,  $m$ , and  $n$ . These parameters are usually derived from borehole measurements and core data but are not available for the Hikurangi Margin due to the lack of nearby drill sites. To derive a suitable parameter set for Opouawe Bank we looked at the range of parameters used in other drilled and surveyed gas hydrate areas at Blake Ridge, ODP 164 [Collett and Ladd, 2000]; Hydrate Ridge, ODP 204 [Tréhu et al., 2006]; and Northern Cascadia Margin, IODP 311 [Expedition 311 Scientists, 2006].

### 5.1. Pore Water Resistivity

Pore water resistivity mainly depends on temperature and salinity. Salinity depth profiles are usually derived from interstitial waters and generally decrease with sediment depth. During gas hydrate formation, salt ions are excluded from the hydrate structure, causing an increase in the surrounding pore water salinity. As the salt diffusivity is generally very low, pore water may remain very conductive (above seawater conductivity) within zones of high hydrate concentration [Liu and Flemings, 2007]. This would have an opposing effect on the formation resistivity and in fact could mean that the calculated gas/gas hydrate saturation would be even higher if a higher pore water salinity is taken into account. However, the effect becomes smaller with increasing saturation, as less pore space is available.

In order to estimate a pore water resistivity depth profile for Opouawe Bank, we used the relationship in equation (8) by Von Herzen et al. [1983] which has been also used by Goswami et al. [2015] at Vestnesa Ridge, west of Spitsbergen.

$$\rho_w = \left( \frac{\sigma_0 + T [^{\circ}\text{C}]}{k} \right)^{-1} \quad (8)$$

where  $\sigma_0$  is the seawater conductivity and  $k$  is the gradient assuming a linear relationship between conductivity and temperature.

Using equation (8) with a bottom seawater conductivity of  $\sigma_0=3$  S/m measured with the CTD sensor, an average geothermal gradient of 40 mK/m measured with temperature sensors in shallow sediments at a transect outside the seeps at Opouawe Bank [Bialas et al., 2007], and a somewhat steeper gradient than Von Herzen et al. [1983] of  $k = 15$  we obtain a pore water resistivity profile for Opouawe Bank with decreasing values from 0.31  $\Omega\text{m}$  at the seafloor to 0.24  $\Omega\text{m}$  at 300 mbsf. This is in agreement with pore water resistivity profiles measured at Blake Ridge [Collett and Ladd, 2000] (Figure S6).

### 5.2. Porosity

Porosity data from Opouawe Bank are only available from four gravity cores along a short transect across South Tower with values between 60% and 50% within the first 4 mbsf [Schwalenberg et al., 2010a].

**Table 1.** Archie Coefficients Used for Gas Hydrate Saturation Estimates at Blake Ridge [Collett and Ladd, 2000], Hydrate Ridge [Tréhu et al., 2006], Cascadia Margin [Expedition 311 Scientists, 2006], and for Opouawe Bank

Region	$a$	$m$	$n$
Blake Ridge, ODP 164	1.05	2.56	1.9386
Hydrate Ridge, ODP 204	1.0	2.8	1.9386
Cascadia Margin, IODP 311	1.0	2.2–2.6	2.0
Opouawe Bank	1.0	2.4	2.0

Porosity depth profiles derived from density logs and core samples at Hydrate Ridge (ODP 204 [Riedel et al., 2006]) and Northern Cascadia Margin (IODP 311 [Expedition 311 Scientists, 2006]) typically decrease from ~60% to ~40% within the first 300 mbsf. To derive saturation estimates for Opouawe Bank we used background porosity profiles within this range.

### 5.3. Archie Coefficients

The choice of proper Archie coefficients and the general use of Archie's law to estimate gas hydrate saturations from electrical resistivity data have been widely discussed and have been found to be practical for porous and sandy sediments. Jackson et al. [1978] found values for  $m$  between 1.4 and 1.9 by using natural and artificial marine sediment samples in laboratory experiments. However, most sets of Archie coefficients have been derived from in situ borehole logs and core data. The constant  $a$  is often set to 1.0. The cementation factor  $m$  generally increases with depth as the pore space is changing in tortuosity.  $a$  and  $m$  are typically derived for background sediment intervals containing no gas or gas hydrate. The saturation factor  $n$  is often set equal to the cementation factor  $m$  but can be much higher in regions of high gas hydrate concentration [Spangenberg, 2001].

In Table 1 we list Archie coefficients which were used for saturation estimates at three other drilled gas hydrate areas. In the absence of any constraints from drilling we used a set of Archie coefficients with  $a=1$ ,  $n=2$ , and  $m=2.4$  for Opouawe Bank which is within the range of Archie parameters found at the other gas hydrate areas and results in saturation estimates closest to 0 for the background sediments away from the seeps. Note, the dependence on  $m$  decreases as resistivity and saturation estimates increase.

Aside from the dependence on the proper choice of Archie's coefficients, we can estimate the saturation below the seeps, assuming that the sediment lithology does not change between background and seeps. The saturation estimates are then considered as additional gas/gas hydrate saturations which do not exclude that some amount of hydrate is present in the background sediments.

### 5.4. Saturation Estimates at Opouawe Bank

In Figure 6 we show apparent saturation estimates calculated with equation (5) from the apparent resistivity profiles in Figure 3 using decreasing porosities from 55 to 48% and pore water resistivities declining from 0.31 to 0.28  $\Omega\text{m}$  with increasing receiver offsets and Archie coefficients  $a=1$ ,  $m=2.4$ , and  $n=2$ . At the seeps the saturations can be as high as 60–80% of the pore volume and small or close to 0% away from the seeps.

In Figure 7 we calculate saturation estimates from the 2-D resistivity models in Figure 5 according to equation (5). Therein we use a similar porosity gradient decreasing from 58% at the seafloor to ~50% at 300 mbsf, a pore water resistivity profile derived from equation (8), and the same set of Archie coefficients as in Figure 6 with  $a=1$ ,  $m=2.4$ , and  $n=2$ .

Saturations rise up to 80% beneath the western seep sites which is in agreement with the apparent saturations in Figure 6. Negative saturations occurring at deeper model parts of profile P2 are attributed to our simplified assumption that the lithology does not change between seeps and background sediments, and thus, we can use the same set of Archie parameters. Saturations of 10 to 20% at intermediate depths in the background sediments at profile meters 5000–8000 of profiles P1 and P2 are caused by the resistive layer in the 2-D models in Figure 5 and could be caused by lithology changes or even a gas hydrate layer of moderate concentration.

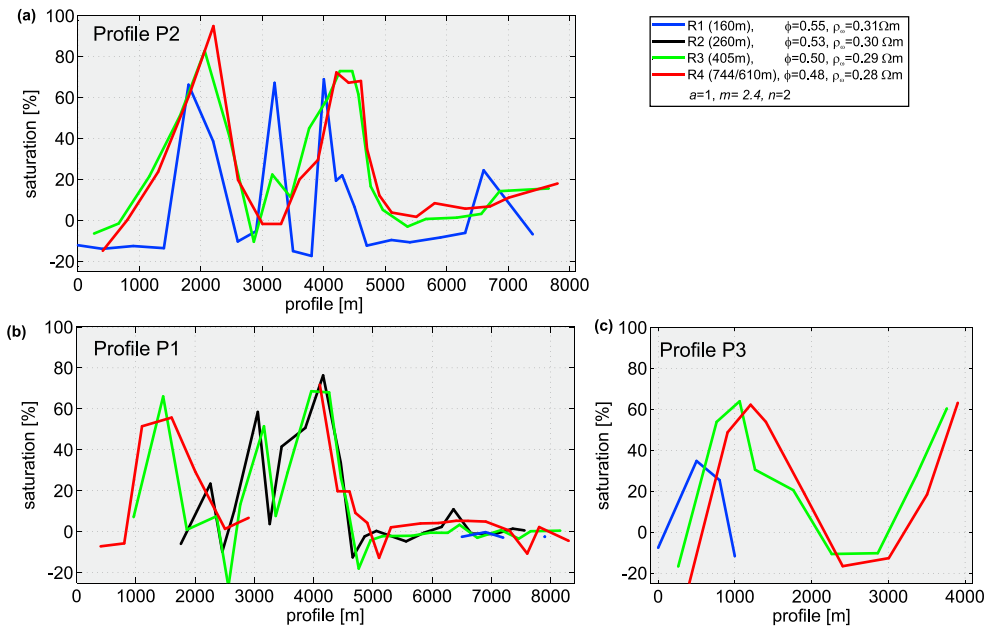


**Figure 6.** Saturation estimates calculated with equation (5) by using the apparent resistivity profiles in Figure 3, decreasing porosities and pore water resistivities with depth, and Archie parameters as shown in the legend. Average saturations are up to 60–80% at the seeps and small or close to 0% away from the seeps.

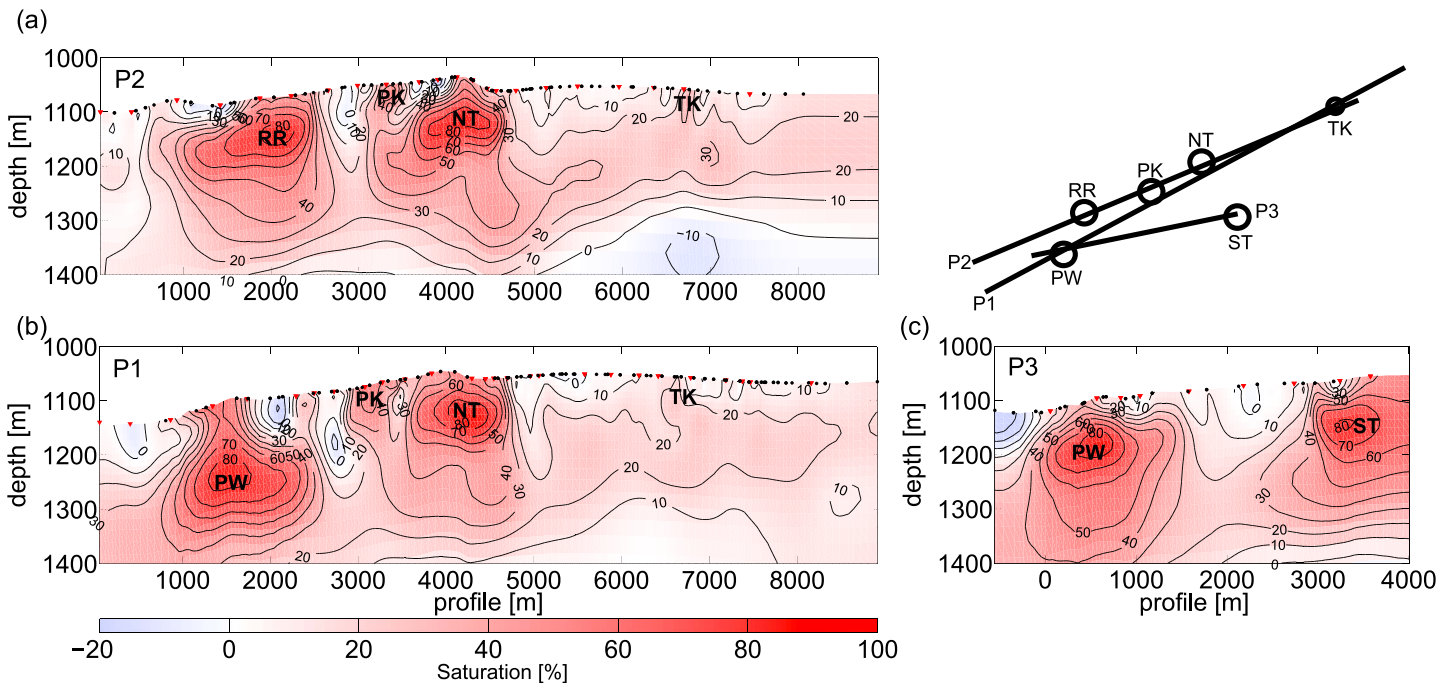


**Figure 7.** Saturation estimates derived from the 2-D models in Figure 5 by using equation (5), a linear porosity gradient from 58% at the seafloor to ~50% at 300 mbsf, a pore water resistivity profile derived from equation (8), and Archie parameter ( $a = 1$ ,  $m = 2.4$ ,  $n = 2$ ). Below the seeps, saturations are up to 80%. Lower resistivities away from the seeps result in saturation estimates in the order of 10–20% and are more sensitive to the chosen porosity and pore water resistivity profile but could also indicate a lower gas hydrate concentration. The seep sites are Takahe (TK), North Tower (NT), Pukeko (PK), Riririro (RR), Piwakawaka (PW), and South Tower (ST).

## 6. Comparing Seismic and CSEM

High-resolution 3-D MCS data (P-cable) and a 2-D MCS line have been acquired in the same target area at Opouawe Bank [Koch *et al.*, 2016] (Figure 1). In Figure 8 we combine the CSEM profiles with the corresponding seismic profiles. CSEM profile P1 is almost coincident with the 2-D MCS line which is therefore used. For profiles P2 and P3 the corresponding depth-migrated seismic lines have been extracted from the 3-D volume.

The profiles show a very good agreement between resistivity anomalies and high seismic amplitude anomalies below the western seep sites. The seismic sections also show vertical conduits with reduced amplitudes and wipe-out zones [Koch *et al.*, 2016; Krabbenhoef *et al.*, 2013]. The resistivity anomalies seem to be clearly separated from each other which is also supported by the seismic images showing layered sedimentation between the individual conduits. In the shallow sediments the gas migration pathways appear as circular structures with various amplitude anomalies also accompanied by gas-controlled doming of seafloor sediments [Koch *et al.*, 2015]. The highest resistivities have been derived at depth where seismic conduits merge into zones of high amplitude reflections (HARs) below the seeps (Riroriro and North Tower on profile P2, Piwakawaka and North Tower on profiles P1, and Piwakawaka and South Tower on profile P3). In some cases HARs seem to enclose the areas of highest resistivity (Riroriro on P2 and Piwakawaka on P1). At Pukeko (profiles P1 and P2), resistivities are highest close to the seafloor.

Takahe seep at profile meter 6800 on profiles P1 and P2 differs from the western seeps. It is seismically characterized by a narrow vertical conduit terminating with high amplitude reflections near the seafloor [Netzeband *et al.*, 2010; Koch *et al.*, 2016] but shows only slightly elevated resistivities on profile P2 in Figure 8b. However, seafloor venting [Greinert *et al.*, 2010], shallow gas hydrate samples [Schwalenberg *et al.*, 2010a; Bialas, 2011], and bacterial mats but no distinctive cold seep communities and no carbonate outcrops have been observed at Takahe [Bowden *et al.*, 2013], indicating that this may be an active and younger seep site where large amounts of gas hydrate have not yet accumulated.

## 7. Interpretation

Marine CSEM data reveal highly anomalous resistivity zones within the first 300 m of the gas hydrate stability zone at Opouawe Bank. Resistivity values in excess of 50  $\Omega\text{m}$  are among the highest derived from marine CSEM data so far. The zones of highest resistivity occur beneath a series of active seafloor vents aligned along the ridge crest. Below the vents, seismic conduits terminate in high amplitude reflections (HARs) at intermediate depths between 75 and 100 mbsf. These conduits indicate focused upward flow of free gas from below the BSR into the GHSZ [Koch *et al.*, 2016]. Between the seeps, resistivities have normal background values of typical shallow seafloor sediments between 1 and 2  $\Omega\text{m}$ , and seismic stratigraphy shows normal layering.

The observation of gas migration pathways, HARs, and extended resistivity anomalies suggests the coexistence of gas hydrate and free gas within the GHSZ at Opouawe Bank. Carbonates are also electrically resistive and have been observed at the seafloor at the western seep sites [Klaucke *et al.*, 2010]. However, the outcrops are patchy and seem to have no depth extent.

From electrical resistivity alone we cannot distinguish between free gas and gas hydrate. High amplitude reflections can be also caused by both patches of free gas and gas hydrate accumulations. Liu and Flemings [2006, 2007] list three mechanisms how free gas can be transported through the gas hydrate stability field: (i) rapid gas flow causing that equilibrium conditions are not present due to kinetic effects; (ii) depletion of water while gas is supplied in excess of its proportion in hydrate; and (iii) upward perturbation of the pressure-temperature boundary by advecting warm fluids, capillary effects in fine-grained sediments, or high pore water salinity linked to massive hydrate formation leading to three-phase equilibrium of water, hydrate, and free gas [Liu and Flemings, 2006]. The first mechanism was used by Torres *et al.* [2004] and Haeckel *et al.* [2004] to explain chloride enrichment, massive gas hydrate formation, and methane transport at southern Hydrate Ridge. At Opouawe Bank, chloride profiles are only available from a few gravity cores showing no chloride enhancement within the first 5 mbsf [Bialas *et al.*, 2007, Koch *et al.*, 2016]. We can also rule out the second point: depletion of water, as water should be available in excess in the wet sediments of the accretionary wedge [Barnes *et al.*, 2010]. Also, the BSR-derived regional heat flow of 35–42  $\text{mW/m}^2$  is generally low [Henrys *et al.*, 2003].



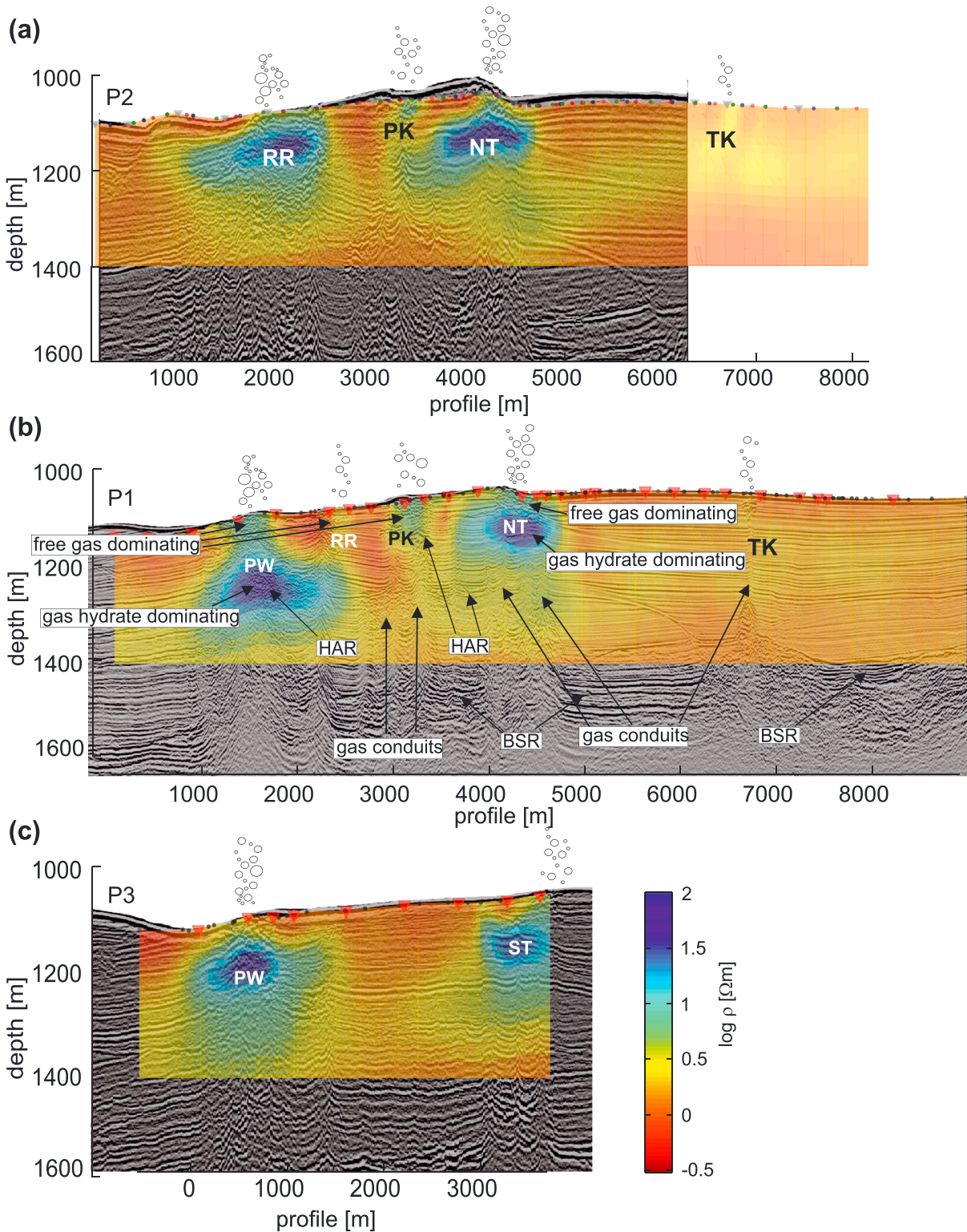


**Figure 8.** The 2-D CSEM models in Figure 5 have been superimposed on the corresponding 2-D depth-converted lines extracted from the 3-D seismic volume (see Figure 1 for location). CSEM profile P1 almost coincides with the 2-D MCS line which is used in this case. The zones of highest resistivity correlate with high amplitude reflections (HARs) located on top of narrow vertical gas conduits, suggesting the coexistence of gas hydrate and free gas within the GHSZ. At intermediate depth within the areas of highest resistivity, gas hydrate may be the dominating constituent, while free gas is prevailing closer to the seafloor, as seismic data, seafloor venting, and resistivity pattern suggest. The seep sites are Takahe (TK), North Tower (NT), Pukeko (PK), Riroriro (RR), Piwakawaka (PW), and South Tower (ST).

Liu and Flemings [2006] demonstrated that the salinity needed for three-phase equilibrium where all phases coexist within the GHSZ requires high hydrate saturations of up to 70%. This would mean that the high resistivity areas at depth from 50 to 200 mbsf are dominated by concentrated gas hydrate. Free gas is likely also present in the central part of the anomalies as seismic data suggest. Massive hydrate formation would increase pore water salinity due to exclusion of salt which would subsequently reduce the formation resistivity. A simple calculation by using equation (5) reveals that reducing the pore water resistivity from, e.g., 0.3  $\Omega$ m to 0.15  $\Omega$ m, would imply an increase in saturation of less than 5% for the high resistivities (>50  $\Omega$ m) derived below the Opouawe Bank seep sites. In other words, there would be simply not enough pore space left, that pore water freshening has a significant impact on the gas/gas hydrate saturation estimates.

Below 100–200 mbsf gas transport is confined to the narrow elongated conduits [Koch, 2016] and gas hydrate saturations are low, as lower resistivities and saturation estimates show. Here the reaction front of three phase equilibrium described by Liu and Flemings [2006] has already moved upward.

At shallow depth, where the areas of high resistivity and the seismic conduits reach the seafloor, free gas may be prevailing as seafloor doming [Koch et al., 2015] and active seafloor venting suggest.

Similar situations of high resistivity anomalies within the GHSZ corresponding to seismically inferred seep sites have been reported by Goswami et al. [2015] on Vestnesa Ridge west of Spitsbergen, Weitemeyer et al. [2011] on Southern Hydrate Ridge, and Schwalenberg et al. [2005] on the Northern Cascadia Margin. Together with our results from Opouawe Bank, these studies support the concept of gas hydrate sweet spots in areas of high fluid flow and gas venting as suggested by, e.g., Liu and Flemings [2007], Boswell and Collett [2011], and Piñero et al. [2013]. Insight from such experiments should be easily transferred and applied to other seep site areas within the gas hydrate stability field. However, more case studies including constraints on the physical parameters from drilling are required to provide ground-truthing of the free gas/gas hydrate distribution below the seeps.

## 8. Conclusions

1-D and 2-D inversion of marine CSEM data showed that significant amounts of gas hydrate may have formed at intermediate depth below a number of methane seep sites at Opouawe Bank on the southern Hikurangi Margin. The areas of highest resistivities correlate with patches of high amplitude reflections in MCS data and are located around seismically inferred narrow conduits along which free gas is transported upward into the gas hydrate stability field. Gas hydrate and free gas likely coexist within the anomalous areas. Free gas may be driven by focused gas flow and three-phase equilibrium of water, hydrate, and gas. Saturation estimates derived with Archie's law are high, up to 80% in the central parts of the anomalies. We believe gas hydrate is the dominating phase, but the share in free gas within these zones is not clear from our analysis. Close to the seafloor hydrate may become less stable and free gas migrates to the seafloor where active venting has been observed.

Connecting marine CSEM and MCS data is demonstrably effective to assess gas and gas hydrate accumulations in the subsurface. The seafloor-towed electric dipole-dipole system HYDRA has shown great use for detailed studies of closely spaced seep sites and related gas hydrate accumulations. Combining resistivity volumes and their distributions with MCS imaging documents their relationship with gas migration structures. Thus, the conclusions about potential gas and gas hydrate reservoirs are highly improved.

## References

- Archie, G. (1942), The electrical resistivity log as an aid in determining some reservoir characteristics, *Trans. AIME*, 146(01), 54–62.
- Attias, E., K. Weitemeyer, T. A. Minshull, A. I. Best, M. Sinha, M. Jegen-Kulcsar, S. Hölz, and C. Berndt (2016), Controlled-source electromagnetic and seismic delineation of subseafloor fluid structures in a gas hydrate province offshore Norway, *Geophys. J. Int.*, 206, 1093–1110, doi:10.1093/gji/ggw188.
- Barnes, P. M., G. Lamarche, J. Bialas, S. Henrys, I. Pecher, G. L. Netzeband, J. Greinert, J. J. Mountjoy, K. Pedley, and G. Crutchley (2010), Tectonic and geological framework for gas hydrates and cold seeps on the Hikurangi subduction margin, New Zealand, *Mar. Geol.*, 272(1–4), 26–48.
- Bialas, J., J. Greinert, P. Linke, and O. Pfannkuche (Eds.) (2007), RV SONNE cruise report SO191—New vents “Puaretanga Hou”, 11.01. - 23.03.2007, Wellington - Napier - Auckland, (Cruise Report No. 09), Kiel, Germany. Berichte aus dem Leibniz-Institut für Meereswissenschaften an der Christian-Albrechts-Universität zu Kiel, ISSN Nr.: 1614–6298.

### Acknowledgments

We thank the captain and crew of R/V SONNE cruise SO214 for excellent technical support. Martin Engels and Joachim Deppe have been indispensable in CSEM instrument preparations and during the cruise. Martin Engels is also thanked for setting up the Matlab<sup>®</sup> processing scripts. Reza Mir and Suzannah Toulmin helped in all CSEM survey activities. Dennis Rippe, Stephanie Koch, and the CSEM survey of the NEMESYS project were financially supported by BMBF grant 03G0214. Katrin Schwalenberg wishes to thank the crew of R/V Kaharoa (NIWA, NZ) who helped recovering the CSEM instrument and data which got lost during cruise SO214. Finally, we thank the Associate Editor, an anonymous reviewer, and Sebastian Hölz for their helpful comments which considerably improved the content of the paper. Metadata of cruise SO214 are available from SeaDataNet.org.

- Bialas, J. (Ed.) (2011), RV SONNE cruise report SO214—NEMESYS, 09.03.-05.04.2011, Wellington - Wellington, 06.-22.04.2011, Wellington – Auckland (Cruise Report No. 47), Kiel, Germany. Berichte aus dem Leibniz-Institut für Meereswissenschaften an der Christian-Albrechts-Universität zu Kiel, ISSN Nr.: 1614–6298.
- Boswell, R., and T. S. Collett (2011), Current perspectives on gas hydrate resources, *Energy Environ. Sci.*, *4*, 1206–1215.
- Bowden, D. A., A. A. Rowden, A. R. Thurber, A. R. Baco, L. A. Levin, and C. R. Smith (2013), Cold seep epifaunal communities on the Hikurangi Margin, New Zealand: Composition, succession, and vulnerability to human activities, *PLoS One*, *8*(10), e76869, doi:10.1371/journal.pone.0076869.
- Cheesman, S. J., R. N. Edwards, and A. D. Chave (1987), On the theory of sea-floor conductivity mapping using transient electromagnetic systems, *Geophysics*, *52*(2), 204–217.
- Collett, T. S., and J. Ladd (2000), Detection of gas hydrate with downhole logs and assessment of gas hydrate concentrations (saturations) and gas volumes on the Blake Ridge with electrical resistivity log data, in *Proceedings of the Ocean Drilling Program, Scientific Results*, vol. 164, edited by C. K. Paul et al., pp. 179–191.
- Collett, T. S., A. H. Johnson, C. C. Knapp, and R. Boswell (2009), Natural gas hydrates: A review, in *Natural Gas Hydrates—Energy Resource Potential and Associated Geologic Hazards*, AAPG Memoir, vol. 89, edited by T. Collett et al., pp. 146–219, AAPG, Tulsa, Okla., and U.S. Department of Energy (NETL), doi:10.1306/13201101M891602.
- Commer, M., and G. A. Newman (2008), New advances in three-dimensional controlled-source electromagnetic inversion, *Geophys. J. Int.*, *172*, 513–535, doi:10.1111/j.1365-246X.2007.03663.x.
- Constable, S. C., R. L. Parker, and C. G. Constable (1987), Occam's inversion: A practical algorithm for generating smooth models from electromagnetic sounding data, *Geophysics*, *52*, 289–300, doi:10.1190/1.1442303.
- Constable, S., P. K. Kannberg, and K. Weitemeyer (2016), Vulcan: A deep-towed CSEM receiver, *Geochem. Geophys. Geosyst.*, *17*, 1042–1064, doi:10.1002/2015GC006174.
- Cook, A. E., B. I. Anderson, A. Malinverno, S. Mrozewski, and D. S. Goldberg (2010), Electrical anisotropy due to gas hydrate-filled fractures, *Geophysics*, *75*(6), 173–185, doi:10.1190/1.3506530.
- Davy, B., and R. Wood (1994), Gravity and magnetic modelling of the Hikurangi Plateau, *Mar. Geol.*, *118*(1–2), 139–151.
- Dumke, I., I. Klauke, C. Berndt, and J. Bialas (2014), Sidescan backscatter variations of cold seeps on the Hikurangi Margin (New Zealand): Indications for different stages in seep developments, *Geo-Mar. Lett.*, doi:10.1007/s00367-014-0361-7.
- Edwards, R. N. (1997), On the resource evaluation of marine gas hydrate deposits using sea-floor transient electric dipole-dipole methods, *Geophysics*, *62*(1), 63–74.
- Edwards, R. N. (2005), Marine controlled source electromagnetics: Principles, methodologies, future commercial applications, *Surv. Geophys.*, *26*, 675–700.
- Ellis, M., R. Evans, D. Hutchinson, P. Hart, J. Gardner, and R. Hagen (2008), Electromagnetic surveying of seafloor mounds in the northern Gulf of Mexico, *Mar. Pet. Geol.*, *25*(9), 960–968, doi:10.1016/j.marpetgeo.2007.12.006.
- Expedition 311 Scientists (2006), Sites U1325, U1327, U1328 and U1329, in *Proceedings of IODP*, vol. 311, edited by M. Riedel et al., pp. 1–136, Integrated Ocean Drilling Program Management International, Inc., Washington, D. C., doi:10.2204/iodp.proc.311.107.2006.
- Greinert, J., K. Lewis, J. Bialas, I. Pecher, A. Rowden, D. Bowden, M. De Batist, and P. Linke (2010), Methane seepage along the Hikurangi Margin, New Zealand: Overview of studies in 2006 and 2007 and new evidence from visual, bathymetric and hydroacoustic investigations, *Mar. Geol.*, *272*(1–4), 6–25.
- Goswami, B. K., K. A. Weitemeyer, T. A. Minshull, M. C. Sinha, G. K. Westbrook, A. Chabert, T. J. Henstock, and S. Ker (2015), A joint electromagnetic and seismic study of an active pockmark within the hydrate stability field at the Vestnesa Ridge, West Svalbard margin, *J. Geophys. Res. Solid Earth*, *120*, 6797–6822, doi:10.1002/2015JB012344.
- Goto, T., et al. (2008), A marine deep-towed DC resistivity survey in a methane hydrate area, Japan Sea, *Explor. Geophys.*, *39*, 52–59.
- Haeckel, M., E. Suess, K. Wallmann, and D. Rickert (2004), Rising methane gas bubbles form massive hydrate layers at the seafloor, *Geochim. Cosmochim. Acta*, *68*, 4335–4345.
- Hashin, Z., and S. Shtrikman (1962), A variational approach to the theory of the effective magnetic permeability of multiphase materials, *J. Appl. Phys.*, *33*, 3125–3131.
- Henrys, S., S. Ellis, and C. Uruski (2003), Conductive heat flow variations from bottom simulating reflectors on the Hikurangi Margin. N. Z., *Geophys. Res. Lett.* *30*(2), 1065, doi:10.1029/2002GL015772.
- Hoerd, A., and C. Scholl (2004), The effect of local distortions on time-domain electromagnetic measurements, *Geophysics*, *69*(1), 87–96, doi:10.1190/1.1649378.
- Jackson, P., D. Smith, and P. Stanford (1978), Resistivity-porosity-particle shape relationships for marine sands, *Geophysics*, *43*(6), 1250–1268.
- Katz, H. R. (1982), Evidence for gas hydrates beneath the continental slope, East Coast, North Island, New Zealand. N.Z., *J. Geol. Geophys.*, *25*, 193–199.
- Klauke, I., W. Weinrebe, C. J. Petersen, and D. Bowden (2010), Temporal variability of gas seeps offshore New Zealand: Multi-frequency geoaoustic imaging of the Wairarapa area, Hikurangi Margin, *Mar. Geol.*, *272*, 49–58.
- Koch, S., C. Berndt, J. Bialas, M. Haeckel, G. Crutchley, C. Papenberg, D. Klaeschen, and J. Greinert (2015), Gas-controlled seafloor doming, *Geology*, doi:10.1130/G36596.1.
- Koch, S., H. Schroeder, M. Haeckel, C. Berndt, J. Bialas, C. Papenberg, D. Klaeschen, and A. Plaza-Faverola (2016), Gas migration through Opuawe Bank at the Hikurangi Margin offshore New Zealand, *Geo-Mar. Lett.*, doi:10.1007/s00367-016-0441.
- Koch, S. (2016), Fluid migration at Opuawe Bank offshore New Zealand, Doctoral Thesis at Christian-Albrechts-Universität Kiel, 111 pp. [Available at [http://macau.uni-kiel.de/receive/dissertation\\_diss\\_00019017](http://macau.uni-kiel.de/receive/dissertation_diss_00019017).]
- Krabbenhoef, A., J. Bialas, I. Klauke, G. Crutchley, C. Papenberg, and G. L. Netzeband (2013), Patterns of subsurface fluid-flow at cold seeps: The Hikurangi Margin, offshore New Zealand, *Mar. Pet. Geol.*, *39*, doi:10.1016/j.marpetgeo.2012.09.008.
- Kvenvolden, K. A. (1993), Gas hydrates—Geological perspectives and global change, *Rev. Geophys.*, *31*, 173–187, doi:10.1029/93RG00268.
- Lewis, K. B., and B. A. Marshall (1996), Seep faunas and other indicators of methane-rich dewatering on New Zealand convergent margins. N.Z., *J. Geol. Geophys.*, *39*, 181–200.
- Liu, X., and P. B. Flemings (2006), Passing gas through the hydrate stability zone at Southern Hydrate Ridge, offshore Oregon, *Earth Planet. Sci. Lett.*, *241*, 211–226, doi:10.10216/j.epsl.2005.10.026.
- Liu, X., and P. B. Flemings (2007), Dynamic multiphase flow model of hydrate formation in marine sediments, *J. Geophys. Res.*, *112*, B03101, doi:10.1029/2005JB004227.
- Luo, M., A. W. Dale, L. Haffert, M. Haeckel, S. Koch, G. Crutchley, H. De Stigter, D. Chen, and J. Greinert (2016), A quantitative assessment of methane cycling in Hikurangi Margin sediments (New Zealand) using geophysical imaging and biogeochemical modeling, *Geochem. Geophys. Geosyst.*, *17*, 4817–4835, doi:10.1002/2016GC006643.



- Netzeband, G., A. Krabbenhoef, M. Zillmer, C. J. Petersen, C. Papenberg, and J. Bialas (2010), The structures beneath submarine methane seeps: Seismic evidence from Opuawe Bank, Hikurangi Margin, New Zealand, *Mar. Geol.*, *272*, 59–70.
- Marquardt, D. W. (1963), An algorithm for least-squares estimation of nonlinear parameters, *J. Soc. Ind. Appl. Math.*, *11*, 431–441.
- Milkov, A. V. (2004), Global estimates of hydrate-bound gas in marine sediments: How much is really out there?, *Earth Sci. Rev.*, *66*, 183–197.
- Paull, C. K., R. Matsumoto, P. J. Wallace, and W. P. Dillon (Eds.) (2000), *Proceedings of the Ocean Drilling Program, Scientific Results*, vol. 164, pp. 1–8, Ocean Drilling Program, College Station, Tex., doi:10.2973/odp.proc.ir.164.1996.
- Pecher, I. A., S. A. Henrys, and H. Zhu (2004), Seismic images of gas conduits beneath vents and gas hydrates on Ritchie Ridge, Hikurangi Margin, New Zealand, *J. Geol. Geophys.*, *47*, 275–279.
- Piñero, E., M. Marquardt, C. Hensen, M. Haeckel, and K. Wallmann (2013), Estimation of the global inventory of methane hydrates in marine sediments using transfer functions, *Biogeosciences*, *10*, 959–975, doi:10.5185/bg-10-959-2013.
- Plaza-Faverola, A., D. Klaeschen, P. Barnes, I. Pecher, S. Henrys, and J. Mountjoy (2012), Evolution of fluid expulsion and concentrated hydrate zones across the southern Hikurangi subduction margin, New Zealand: An analysis from depth migrated seismic data, *Geochem. Geophys. Geosyst.*, *13*, Q08018, doi:10.1029/2012GC004228.
- Riedel, M., G. D. Spence, N. R. Chapman, and R. D. Hyndman (2002), Seismic investigations of a vent field associated with gas hydrates, offshore Vancouver Island, *J. Geophys. Res.* *107*(B9), 2200, doi:10.1029/2001JB000269.
- Riedel, M., T. S. Collett, and R. D. Hyndman (2005), Gas hydrate concentration estimates from chlorinity, electrical resistivity and seismic velocity, *Geol. Surv. of Canada, Open File Rep.*, *4934*, 28 pp.
- Riedel, M., P. Long, C. S. Liu, P. Schultheiss, T. Collett, and ODP Leg 204 Shipboard Scientific Party (2006), Physical properties of near surface sediments at Southern Hydrate Ridge: Results from ODP Leg 204, in *Proceedings of the ODP, Scientific Results*, vol. 204, edited by A. M. Tréhu et al., pp. 1–29, Ocean Drilling Program, College Station, Tex., doi:10.2973/odp.proc.sr.204.104.2006.
- Schwalenberg, K., E. C. Willoughby, R. Mir, and R. N. Edwards (2005), Marine gas hydrate electromagnetic signatures in Cascadia and their correlation with seismic blank zones, *First Break*, *23*, 57–63.
- Schwalenberg, K., M. Haeckel, J. Poort, and M. Jegen (2010a), Evaluation of gas hydrate deposits in an active seep area using marine controlled source electromagnetics: Results from Opuawe Bank, Hikurangi Margin, New Zealand, *Mar. Geol.*, *272*(1–4), 79–88.
- Schwalenberg, K., W. T. Wood, I. A. Pecher, L. J. Hamdan, S. A. Henrys, M. D. Jegen, and R. B. Coffin (2010b), Preliminary interpretation of electromagnetic, heat flow, seismic, and geochemical data for gas hydrate distribution across the Porangahau Ridge, New Zealand, *Mar. Geol.*, *272*, 89–98.
- Schwalenberg, K., and M. Engels (2011), HYDRA—A new towed electromagnetic seafloor system, *Geophys. Res. Abstr.*, EGU General Assembly 2011. vol. 13, EGU2011-12525.
- Shankar, U., and M. Riedel (2014), Assessment of gas hydrate saturation in marine sediments from resistivity and compressional-wave velocity measurements in the Mahanadi Basin, India, *Mar. Pet. Geol.*, *58*, 265–277.
- Spangenberg, E. (2001), Modeling of the influence of gas hydrate content on the electrical properties of porous sediments, *J. Geophys. Res.*, *106*, 6535–6548, doi:10.1029/2000JB900434.
- Torres, M. E., K. Wallmann, A. M. Tre'hu, G. Bohrmann, W. S. Borowski, and H. Tomaru (2004), Gas hydrate growth, methane transport, and chloride enrichment at the southern summit of Hydrate Ridge, Cascadia margin off Oregon, *Earth Planet. Sci. Lett.*, *226*, 225–241.
- Townend, J. (1997), Estimates of conductive heatflow through bottom simulating reflectors on the Hikurangi and southwest Fjordland continental margins. *N. Z. Mar. Geol.*, *141*, 209–220.
- Tréhu, A. M., G. Bohrmann, M. E. Torres, and F. S. Colwell (Eds.) (2006) *Proc. ODP, Sci. Results*, vol. 204, Ocean Drilling Program, College Station, Tex., doi:10.2973/odp.proc.sr.204.2006.
- Von Herzen, R. P., T. J. G. Francis, and K. Becker (1983), *In-Situ Large Scale Electrical Resistivity of Ocean Crust, Hole 504B, Init. Repts. DSDP*, vol. 69, edited by Cann, J. R., et al., pp. 237–244, U.S. Govt. Printing Office, Washington, D. C., doi:10.2973/dsdp.proc.69.106.1983.
- Walcott, R. I. (1978), Present tectonics and late Cenozoic evolution of New Zealand, *Geophys. J. R. Astron. Soc.*, *52*, 137–164.
- Weitemeyer, K. A., S. C. Constable, K. W. Key, and J. P. Behrens (2006), First results from a marine controlled-source electromagnetic survey to detect gas hydrates offshore Oregon, *Geophys. Res. Lett.*, *33*, L03304, doi:10.1029/2005GL024896.
- Weitemeyer, K., and S. Constable (2010), Mapping shallow geology and gas hydrate with marine CSEM surveys, *First Break*, *28*, 97–102.
- Weitemeyer, K. A., S. Constable, and A. M. Trehu (2011), A marine electromagnetic survey to detect gas hydrate at Hydrate Ridge, Oregon, *Geophys. J. Int.*, doi:10.1111/j.1365-246X.2011.05105.x.
- Wood, W. T., P. L. Stoffa, and T. H. Shipley (1994), Quantitative detection of methane hydrate through high-resolution seismic velocity analysis, *J. Geophys. Res.*, *99*, 9681–9695, doi:10.1029/94JB00238.
- Wood, W. T., P. E. Hart, D. R. Hutchinson, N. Dutta, F. Snyder, R. B. Coffin, and J. F. Gettrust (2008), Gas and gas hydrate distribution around seafloor seeps in Mississippi Canyon, Northern Gulf of Mexico, using multi-resolution seismic imaginary, *Mar. Pet. Geol.*, *25*, 952–959.
- Yuan, T., R. D. Hyndman, G. D. Spence, and B. Desmons (1996), Seismic velocity increase and deep-sea gas hydrate concentration above a bottom-simulating reflector on the northern Cascadia continental slope, *J. Geophys. Res.*, *101*, 13,655–13,671, doi:10.1029/96JB00102.
- Yuan, J., and R. N. Edwards (2000), The assessment of marine gas hydrates through electrical remote sounding: Hydrate without a BSR?, *Geophys. Res. Lett.*, *27*, 2397–2400, doi:10.1029/2000GL011585.